View metadata, citation and similar papers at core.ac.uk

brought to you by CORE

provided by Elsevier - Publisher Connector

Journal of Computational and Applied Mathematics 236 (2012) 4623–4634

Contents lists available at SciVerse ScienceDirect

Journal of Computational and Applied Mathematics

journal homepage: www.elsevier.com/locate/cam

Simulation of planar ionization wave front propagation on an unstructured adaptive grid

Fayssal Benkhaldoun [a], Jaroslav Fořt [b], Khaled Hassouni [c], Jan Karel [a,b,*]

[a] LAGA, University Paris 13, 99 Av. J.B. Clement, 93430 Villetaneuse, France

[b] CTU in Prague, Faculty of Mechanical Engineering, Karlovo namesti 13, 121 35 Prague, Czech Republic

[c] LSPM, University Paris 13, 99 Av. J.B. Clement, 93430 Villetaneuse, France

ARTICLE INFO

Article history:
Received 31 July 2011
Received in revised form 10 April 2012

Keywords:
Discharge motion
Numerical simulation
Dynamic mesh adaptation

ABSTRACT

The paper deals with the numerical solution of a basic 2D model of the propagation of an ionization wave. The system of equations describing this propagation consists of a coupled set of reaction–diffusion-convection equations and a Poissons equation. The transport equations are solved by a finite volume method on an unstructured triangular adaptive grid. The upwind scheme and the diamond scheme are used for the discretization of the convection and diffusion fluxes, respectively. The Poisson equation is also discretized by the diamond scheme. Numerical results are presented. We deal in more detail with numerical tests of the grid adaptation technique and its influence on the numerical results. An original behavior is observed. The grid refinement is not sufficient to obtain accurate results for this particular phenomenon. Using a second order scheme for convection is necessary.

© 2012 Elsevier B.V. All rights reserved.

1. Introduction

Non-equilibrium ionization processes (discharges) occur when a neutral gas is exposed to high intensity electric field. They can appear in various forms depending on the electric field and on the pressure and the volume of the medium. We focus on streamers that are filamentary discharges generated by ionization waves. Streamer discharges are used for several applications such as pollutant removal. Many papers deal with the numerical simulation of streamer propagation. They are based on mathematical models of different levels of complexity. Most of these models make use of the hydrodynamic approximation, which leads to a governing system of equations that includes a set of convection–diffusion–reaction equations for charged particles coupled with a stationary Poisson's equation for the electric field.

Depending on the complexity level of the model, the system of governing equations can strongly differ in the formulation of source terms and transport fluxes. For example, the photoionization, which is an important phenomenon from a physical point of view, introduces a significant degree of complexity (see e.g. [1]). It is often treated with a strongly simplified model through a background density of electrons and positive ions.

As far as the numerical simulation of streamer propagation is concerned, the difficulty that has to be overcome comes from the crucial significance of a very narrow region where the variables that govern the physics of the system experience several orders of magnitude of variation.

Many methods used for streamer simulation consider a structured, often Cartesian, grid, e.g. [2–4]. In [2], independent refinement procedures for continuity equations and for Poisson's equation are used to capture the wave front in a Cartesian

* Corresponding author at: CTU in Prague, Faculty of Mechanical Engineering, Karlovo namesti 13, 121 35 Prague, Czech Republic. Tel.: +420 224357439; fax: +420 22492 0677.
E-mail address: jan.karel@fs.cvut.cz (J. Karel).

0377-0427/$ – see front matter © 2012 Elsevier B.V. All rights reserved.
doi:10.1016/j.cam.2012.04.010

grid mesh system. In [4], a hierarchy of refined Cartesian sub-grids is constructed by the parallel PARAMESH library. A refinement criterion that depends on the ratio of the electron density and the electric field intensity is applied locally. In [3], a large dynamic range of local grid refinement (up to 10–12 levels) is presented for a Cartesian grid. Simulations have been also carried out on unstructured meshes using the finite-element approach and an adaptive mesh generator [5], where the adaptation criterion is selected using three indicators, the magnitude of the ionization source term S_e, $|\text{grad } n_e|/n_e$ and the magnitude of the net charge density $\rho = e(n_i - n_e)$. In [6] the authors use an adaptive finite element method where the grid refinement is carried out using error indicators based on the density gradients of charged species. Despite the impressive progress in streamer simulation, there are still many challenging topics to be addressed. Among these, 3D simulations allowing to describe streamer branching or propagation in complex geometries are still needed. As a matter of fact, most of the simulations published in the literature deal with axisymmetric geometries that are often far from the ramified structure of the filamentary discharges observed in practice.

The objective of our work is to develop a method that has the potential to address this challenging issue. The idea is to use a general unstructured grid, which can capture the propagation of a very steep 3D wave front in a straightforward way. In this paper we present the first step of this work where we focus on the development of efficient finite volume numerical schemes and grid adaptation algorithms. In this first step, we consider a 2D case (instead of axisymmetric geometry of a cylindrical streamer) and therefore simulate a periodical planar ionization front. We use a basic minimal model of ionization wave propagation in non-attaching gas as N_2 or Ar [2,3] see part 2. The transport coefficients and source terms in the governing equations are estimated using the expressions published in [7].

It is worthy to mention that using unstructured mesh and suitable grid adaptation algorithm makes the transition from 2D to 3D geometries straightforward, especially when an object oriented programming approach is used.

In the following we briefly mention the minimal discharge model and formulate the test problem. Next we describe the finite volume method on unstructured grid for charged species transport and Poisson's equations. We also describe the adaptive mesh refinement algorithm. In the second part we first study the influence of alternative grid adaptation indicators for the 1st order method in space variables. We focus on the grid quality in the critical regions and on the ability of the algorithm to map efficiently these critical regions with enough grid cells. Then we test the properties of first and second order numerical methods and finally show the efficiency and accuracy of the adaptation algorithm through comparison with results achieved on a uniformly refined mesh in the whole computational domain.

2. Governing equations

We consider the simplest minimal model of discharge motion [2,3]

$$\begin{aligned} &\frac{\partial n_e}{\partial t} + \operatorname{div}\left(n_e \vec{v}_e - D_e \vec{\nabla} n_e\right) = S_e, \\ &\frac{\partial n_i}{\partial t} = S_i^+, \end{aligned} \tag{1}$$

where t is the time, n_e denotes the electron density, n_i the positive ion density, $\vec{v}_e$ the electron drift velocity, D_e the diffusion coefficient. $S_e = S_i^+$ are source terms. The system (1) is coupled with the Poisson's equation for the electric potential V

$$\Delta V = Q, \tag{2}$$

where $Q = -\frac{e}{\epsilon}(n_i - n_e)$, ϵ is the dielectric constant, e the electron charge. The intensity of the electric field is computed by the equation $\vec{E} = -\vec{\nabla} V$. The electron drift velocity $\vec{v}_e$ is a function of the electric field $\vec{E}$ and depends on the ratio $\|\vec{E}\|/N$ where N is the neutral gas density ($N = 2.5 \cdot 10^{19}$ cm^{-3}) [7]

$$\vec{v}_e = -\left[C_1(\vec{E}) \cdot \frac{\|\vec{E}\|}{N} + C_2(\vec{E})\right] \cdot \frac{\vec{E}}{\|\vec{E}\|}. \tag{3}$$

The diffusion coefficient D_e is a function of the electron drift velocity and the electric field [7]

$$D_e = \left[0.3341 \cdot 10^9 \cdot \left(\frac{\|\vec{E}\|}{N}\right)^{0.54069}\right] \cdot \frac{\|\vec{v}_e\|}{\|\vec{E}\|}. \tag{4}$$

The source terms depend on the electron drift velocity and the electron density

$$S_e = \frac{\alpha}{N} \cdot \|\vec{v}_e\| \cdot n_e \cdot N, \tag{5}$$

$$S_i^+ = S_e \tag{6}$$

where the ratio $\frac{\alpha}{N}$ is computed by following formula

$$\frac{\alpha}{N} = C_3(\vec{E}) \cdot \exp\left(\frac{C_4}{\|\vec{E}\|/N}\right). \tag{7}$$

See Appendix (21) for more details.

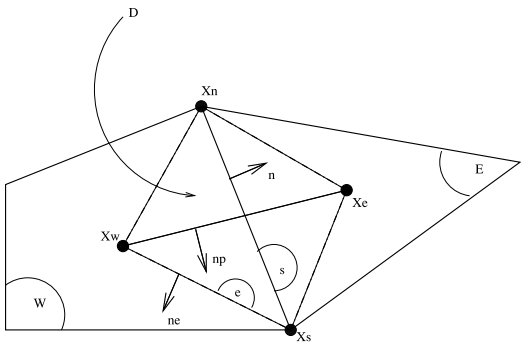

Fig. 1. VF diamond scheme.

3. Numerical method

The equations of the model are discretized using the finite volume method on an unstructured triangular mesh. The time-integration of the transport equations is performed using an explicit scheme. The discretized form of Poisson's equation consists of a linear algebraic system that is solved with a direct method at each time step during the time-integration. We approximate the equation for the *the electron density* by the following finite volume method:

$$\frac{\partial n_e}{\partial t} + \frac{1}{\mu(T)} \oint_{\partial T} n_e \vec{v}_e \vec{n} ds - \frac{1}{\mu(T)} \oint_{\partial T} D_e \vec{\nabla} n_e \vec{n} ds = S_e \tag{8}$$

where $\mu(T)$ is the volume of the cell T, $\vec{n}$ the outward unit normal vector to the faces of the cell T. We approximate the time derivative by a forward difference and the integral along faces of a cell by a second order accurate midpoint formula. We obtain for a cell i

$$\frac{n_{e_i}^{n+1} - n_{e_i}^n}{\Delta t} + \frac{1}{\mu(T_i)} \sum_{j=1}^{m} \oint_{\sigma_{ij}} \left(n_{e_{ij}}^n \vec{v}_{e_{ij}} \vec{n}_{ij} ds_{ij} - D_{e_{ij}} \vec{\nabla} n_{e_{ij}}^n \vec{n}_{ij} ds_{ij} \right) = S_{e_i}, \tag{9}$$

where Δt is the time step, m is number of faces of the cell i, $\vec{n}_{ij}$ is the unit normal vector of the face σ_{ij} (face between a cell T_i and a cell T_j), and ds_{ij} is its length. Other variables denoted by the subscripts ij represent variables on the face σ_{ij}.

3.1. Gradient approximation by finite volume diamond scheme

One must write an estimation of the gradient $\vec{\nabla}_\sigma u$ of a given unknown u on a given cell face σ in order to estimate both the diffusion flux divergence term and the discretized form of Poisson's equation. This is done in the following way: first, one constructs a co-volume D_σ by connecting the barycenters of the cells K and L that share the face σ and its endpoints. Then one assumes that the Gradient is constant on the co-volume D_σ (hence $\vec{\nabla}_\sigma u = \vec{\nabla} u(D_\sigma)$) and, using the Green–Gauss theorem, writes (see Fig. 1):

$$\int_{D_\sigma} \vec{\nabla} u \vec{n} ds = \mu(D_\sigma) \vec{\nabla} u(D_\sigma) = \oint_{\partial D_\sigma} (u, u)^T . \vec{n} ds \tag{10}$$

This resumes in the following formulae for the approximation of the gradient ($|\sigma|$ being the measure of the face σ):

$$\vec{\nabla}_\sigma u = \frac{1}{2\mu(D_\sigma)} \left[(u_L - u_K) |\sigma| \mathbf{n}_{K,\sigma} + (u_N - u_S) |s_\sigma| \mathbf{n}'_\sigma \right]. \tag{11}$$

The values u_N and u_S in vertices N, S are computed by the least square method

$$u_N = \sum_{p=1}^{r(N)} \alpha_p(N) u_p, \qquad u_S = \sum_{p=1}^{r(S)} \alpha_p(S) u_p,$$

where u_p is the value of u in the cell T_p, $r(N)$ ($r(S)$) is the number of cells including vertex N (S), $\alpha_p(N)$ ($\alpha_p(S)$) are weights coming from the least square method.

3.2. Discretization of the convective terms

The convective flux is computed by a simple upwind scheme

$$n_{e_{ij}} = \begin{cases} n_{e_i} & \text{if } (\vec{v}_{e_{ij}} \cdot \vec{n}_{ij}) \geq 0, \\ n_{e_j} & \text{in other case,} \end{cases} \tag{12}$$

with assumption that the normal vector $\vec{n}_{ij}$ is oriented from the cell i to the cell j. Computation of the interface drift velocity $\vec{v}_{e_{ij}}$ will be discussed later (see Eqs. (3.6), (17)).

3.2.1. Second order in space variables for the convection scheme

The upwind scheme has a first order accuracy, which results in a high numerical dissipation that is only partly compensated by grid refinement. This scheme was hence extended using a Van Leer's type MUSCL algorithm together with a Barth–Jesperson limiter in order to achieve a second order accuracy in space.

We introduce in the Eq. (12) $\widetilde{n}_{e_i}, \widetilde{n}_{e_j}$ instead of $n_{e_i},\ n_{e_j}$

$$\widetilde{n}_{e_i} = n_{e_i} + \psi_i(\vec{\nabla} n_{e_i} \cdot \vec{r}_i), \qquad \widetilde{n}_{e_j} = n_{e_j} + \psi_j(\vec{\nabla} n_{e_j} \cdot \vec{r}_j),$$

where $\vec{\nabla} n_{e_i}, \vec{\nabla} n_{e_j}$ are gradients of electron density in cells T_i, T_j. These gradients are computed assuming that the electron density is a piecewise linear function, whose value is n_{e_i} at the center of gravity of T_i. This linear function is computed by a least square method involving all neighboring cells of the vertices of T_i. $\vec{r}_i$ ($\vec{r}_j$) is a vector coming from cell T_i (T_j) center of gravity to face σ_{ij} midpoint. ψ_i (ψ_j) is the Barth–Jesperson limiter function [8].

3.3. Discretization of diffusion terms

For the diffusion term, one writes:

$$\oint_{\sigma_{ij}} D_{e_{ij}} \vec{\nabla} n^n_{e_{ij}} \vec{n}_{ij} ds_{ij} = |\sigma_{ij}| D_{e_{ij}} \vec{\nabla}_{|\sigma_{ij}} n^n_{e_{ij}} \vec{n}_{ij}$$

where $\vec{\nabla}_{|\sigma_{ij}} n^n_{e_{ij}}$ is the approximation of the gradient as presented in Section 3.1, and computation of the diffusion coefficient $D_{e_{ij}}$ is described in the Eq. (17).

3.4. Equation for ion density

The equation for *the ion density* is solved by an explicit Euler method

$$n_i^{n+1} = n_i^n + \Delta t S_i^{+n}. \tag{13}$$

3.5. Poisson's equation

The integration of Poisson's equation over a given cell T gives:

$$\oint_{\partial T} \vec{\nabla} V \vec{n} ds = \int_T Q dv \tag{14}$$

We use a similar finite volume approximation as for diffusive terms in the equation for electron density

$$\sum_{j=1}^{m} \oint_{\sigma_{ij}} \left(\vec{\nabla} V_{ij}^{n+1} \vec{n}_{ij} ds_{ij} \right) \approx \sum_{j=1}^{m} |\sigma_{ij}| \vec{\nabla}_{|\sigma_{ij}} V_{ij}^{n+1} = \mu(T_i) Q_i^{n+1}, \tag{15}$$

this leads to a system of linear equations

$$\boldsymbol{A} \cdot \vec{V}^{n+1} = \vec{Q}^{n+1}. \tag{16}$$

The updated values $n_e^{n+1},\ n_i^{n+1}$ are used for evaluation of the source term in (2). The system of Eq. (16) is solved directly by *LU* decomposition with an implementation for sparse matrices. (We use Intel MKL library solvers.) The coefficients of matrix $\boldsymbol{A}$ in (16) depend only on the grid topology. We recalculate L and U matrices after each new mesh adaptation.

3.6. Electric field, drift velocity and diffusion coefficient computation

One has $\vec{E}^{n+1} = -\text{grad}(V^{n+1})$. We compute components of the intensity of the electric field on cell faces as:

$$E_{x_{ij}} = -\frac{1}{\mu(A_{ij})} \sum_{k=1}^{4} V_k n_{x_k} ds_k, \qquad E_{y_{ij}} = \frac{1}{\mu(A_{ij})} \sum_{k=1}^{4} V_k n_{y_k} ds_k.$$

The electron drift velocity is a function of the electric field and the diffusion coefficient D_e is a function of the electron velocity and the electric field:

$$\vec{v}_{e_{ij}}^{n+1} = f(\vec{E}_{ij}^{n+1}), \qquad D_{e_{ij}}^{n+1} = g(\vec{v}_{e_{ij}}^{n+1}, \vec{E}_{ij}^{n+1}). \tag{17}$$

The values at the center of gravity of a cell T_i are estimated from the average of these values on the associated faces.

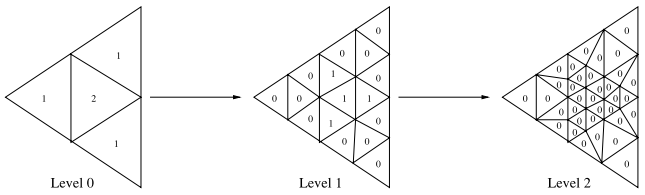

Fig. 2. Mechanism of multi-level mesh refinement.

3.7. Dynamic mesh adaptation

In order to improve the efficiency of the presented finite volume scheme, we have performed a dynamic mesh adaptation to construct a mesh able to capture the stiff gradient of variables in regions of propagating fronts. A similar algorithm has been applied in [9] for adaptive finite volume solution of a combustion system. The algorithm starts by computing some criterion on a fixed coarse reference grid, (e.g. gradient of some unknown), which serves as a guide to make the refinement and unrefinement decisions. The values of the criterion are then scaled into interval $\langle 0, 1\rangle$ which is split into subintervals with prescribed level of adaptation. A list of elements to be refined, their degree of refinement, and those to be unrefined is then established. When each triangle of the reference grid has been subdivided, a grid conformity procedure is applied. In particular the maximum difference of refinement level between neighboring cells cannot exceed one. The values of the unknowns are thereafter conservatively interpolated on the newly adapted grid (see Fig. 2).

4. Numerical experiment presentation

We consider the 2D problem of the discharge propagation in a homogeneous electric field described by (1)–(7). Our domain is a rectangle 1×0.5 cm.

Initial conditions:

$$\begin{aligned} &n_e(x, y, 0) = 10^{16} \cdot e^{-\frac{(x-0.2)^2+(y-0.25)^2}{\sigma^2}} + 10^9\ [\mathrm{cm}^{-3}], \quad \sigma = 0.01, \\ &n_i(x, y, 0) = n_e(x, y, 0). \end{aligned} \tag{18}$$

The initial Gaussian pulse for the electron and the ion densities creates a disturbance in the electric field which is necessary for the initiation of the ionization wave propagation. The background electron and ion with a density of 10^9 substitutes the photoionization phenomenon which is neglected in our simple discharge model. We stop computation at a prescribed time, when the head of discharge is still inside the computational domain. The discharge leaves the computational domain through the right boundary, if the simulation time is sufficiently extended. The periodicity condition for electric field potential on side boundaries is used to simplify the test case. We does not investigate the influence of the side boundary position on the discharge propagation.

Boundary condition:

The left boundary of the domain is a plane anode, the right boundary is a plane cathode. Lower and upper boundaries are periodical boundaries for all unknowns and for the anode and the cathode we prescribe the following boundary condition:

$$\begin{array}{ll} \dfrac{\partial ne}{\partial \vec{n}} = 0 & \text{for } x = 0,\ x = 1, \\ V = 25000\ [\mathrm{V}] & \text{for } x = 0, \\ V = 0\ [\mathrm{V}] & \text{for } x = 1. \end{array} \tag{19}$$

5. Numerical results

The outline of the section is the following: we will first show the results obtained for the discharge propagation and the electron avalanche phenomenon obtained with a second order upwind scheme on adapted grids. A second series of tests will be discussed to show the impact of the adaptation criterion on the results when using a first order scheme. We end by a comparison of results obtained by a first order and a second order upwind scheme for convection, on different uniformly refined grids and on adapted grids.

5.1. Discharge propagation

We first present in Figs. 3 and 4 a result obtained with the second order upwind scheme on a dynamically adapted mesh. The shape and magnitude of velocity vectors fully agrees with the physical mechanism of electron avalanche propagation.

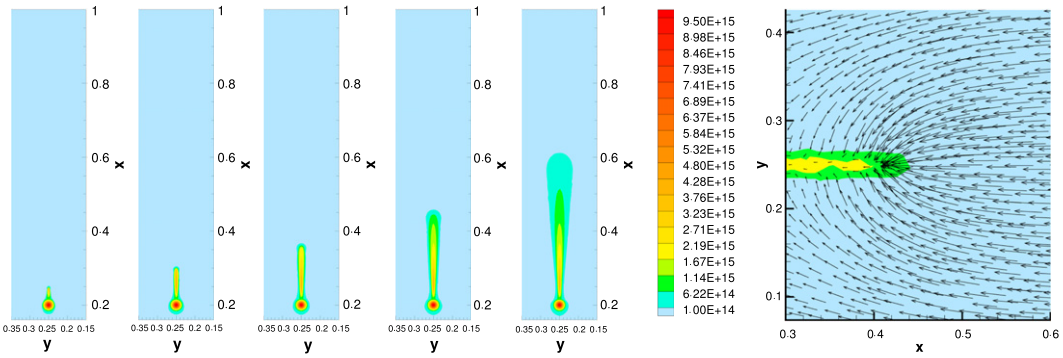

Fig. 3. 2nd order computation: electron density (contour levels) at times $t = 3.859 \cdot 10^{-8}$ s, $t = 4.435 \cdot 10^{-8}$ s, $t = 4.847 \cdot 10^{-8}$ s, $t = 5.25 \cdot 10^{-8}$ s and $t = 5.659 \cdot 10^{-8}$ s (end of computation), 2nd order scheme, adapted grid; electron velocity vectors at a head of a discharge (right).

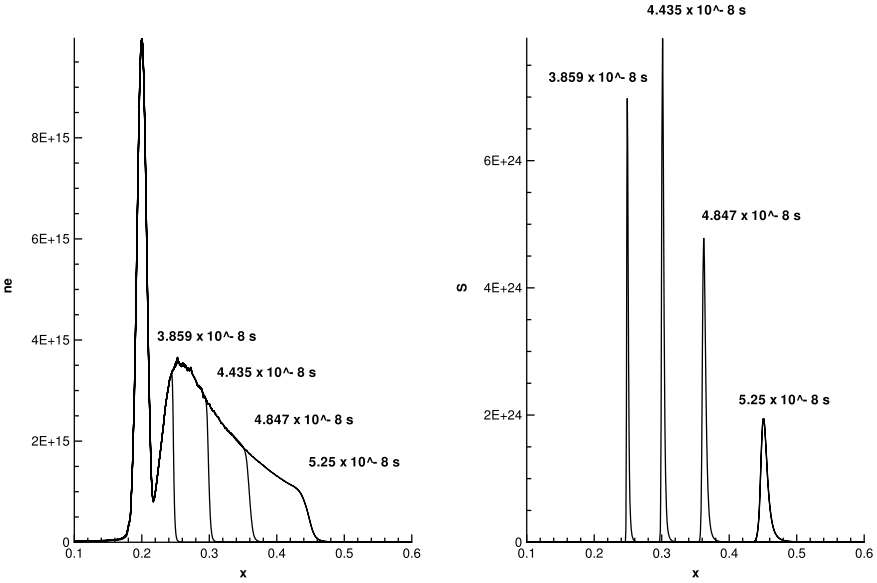

Fig. 4. 2nd order computation: Evolution of electron density (left) and source terms (right) magnitudes, 2nd order scheme, adapted grid.

Table 1
Number of cells, nodes of reference mesh and mesh at $t_{\text{in}} = 3.14 \cdot 10^{-8}$.

	Cells	Nodes
Reference mesh	4700	2424
Mesh at $t_{\text{in}} = 3.14 \cdot 10^{-8}$	9154	4651

5.2. Grid adaptation tests

Test description

All computations are done by the first order scheme on the same reference grid (see Fig. 5) with approximately 5000 triangles. The temporal results achieved on adapted grid at physical time $t_{\text{in}} = 3.14 \cdot 10^{-8}$ s calculated from the initial conditions (18) have been used as a starting approximation (see Table 1).

The choice of t_{in} as a reference time for the grid adaptation procedure was motivated by the fact that for time-values smaller than 34 ns we only observe a space charge build-up and an electric field enhancement. There is no planar wave propagation during this period of time. We compare results achieved at the same physical time $T = 5.25 \cdot 10^{-8}$ s. The number of triangles and nodes in Table 2 means the values on adapted grid at time $t = T$. The CPU time is the relative CPU time necessary for the computation of a solution in time interval $\langle t_{\text{in}}, T \rangle$.

Presentation of the results:

Each computation is presented in a one row. We rotate the computational domain 90° anti-clockwise.

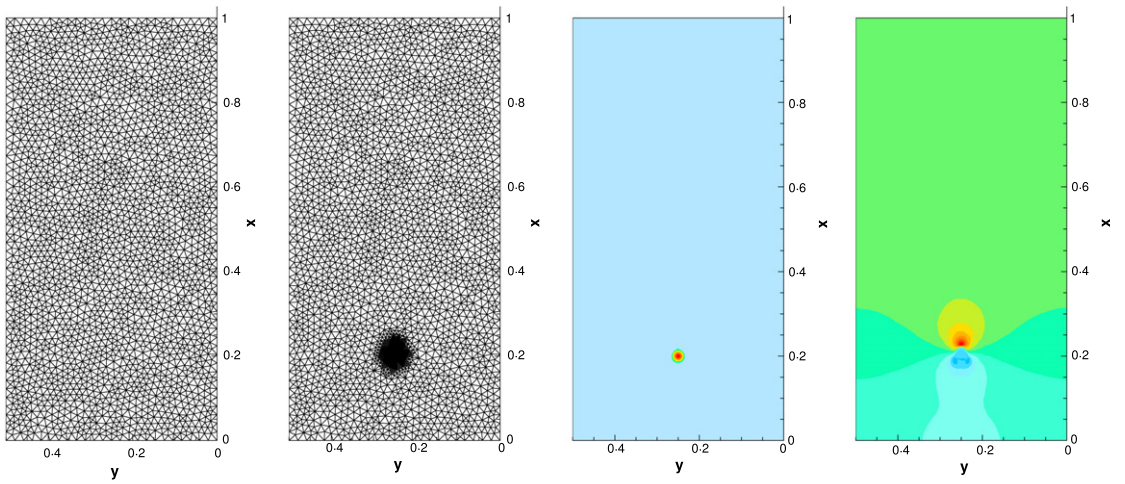

Fig. 5. Reference mesh, mesh, electron density, electric field at $t_{\text{in}} = 3.14 \cdot 10^{-8}$.

Table 2
Number of cells, nodes and CPU time at $t = 5.25 \cdot 10^{-8}$ s.

Adaptation criterion	Cells	Nodes	CPU time
Source terms	11 760	5 954	1
Electron density gradient	16 714	8 431	0.447
Both, Algorithm V1	18 520	9 334	0.716
Both, Algorithm V2	22 422	11 285	1.522

The first and second column shows the isolines of n_e and source term S_e at time T in zoom $\langle 0.15, 0.35\rangle$ horizontally and $\langle 0.16, 1\rangle$ vertically. The adapted grid at time T is plotted in the third column. The relation of adapted grid density and isolines of n_e is shown in the fourth (zoom $\langle 0.18, 0.32\rangle x \langle 0.15, 0.4\rangle$) and fifth columns (zoom $\langle 0.18, 0.32\rangle x \langle 0.4, 0.68\rangle$). The zoom of the adapted grid around the discharge head is plotted together with isolines of S_e in the last sixth column.

Choice of criterion variable.

The first row in Fig. 6 shows results when the magnitude of a source term is chosen as criterion function crit $= S_e$ (case 1, row 1). The second row shows results of case 2 (row 2), when the criterion is based on gradient of n_e, crit $= |\text{grad } n_e|$. Finally we present results of case 3, when both previous criterion are used simultaneously crit $= \max(|\text{grad } n_e|, S_e)$. This is done using two different Algorithms, V1 and V2.

In the version V1 (row 3), one scales both criteria to one (dividing by the maximal value respectively), then constructs a function where the value on each cell is equal to the maximum of these two scaled criterions, this new function is smoothed and scaled once more to one and gives the new criterion.

In the version V2 (row 4), each criterion is smoothed and scaled to one separately and the new criterion for each cell is the maximum of the two obtained values.

Discussion of results.

We can observe that the choice of the variable used to set up the adaptation criterion significantly affects the simulated propagation of the planar ionization wave. This may be clearly seen on the different time variation of the front position and, therefore discharge propagation velocity, obtained between the first two cases. The lower level of grid adaptation in region of high values of the source term S_e brings a smearing of source term and higher propagation speed—typically case 2, partly case 3 version V1. On the other hand the criterion based only on the magnitude of the source term – case 1 – produces too low values of n_e in the discharge path (initial part). We can also observe that only simultaneous use of both variables (case 3) in the grid adaptation criterion produces acceptable results (see also the next paragraphs).

5.3. Grid density and scheme order tests: comparison of 1st and 2nd order schemes for convective term both on uniformly refined grids and on adaptive grids

We deal with the influence of the grid density for both theoretically 1st and 2nd order approximations in space variables. We use the same construction of test case as in the previous subsection.

Test description. The starting approximation is once more the solution at time $t_{\text{in}} = 3.14 \cdot 10^{-8}$ s plotted in Fig. 5. The used grids are meshes obtained by successive refinements of the reference grid using 1–4 levels of refinement.

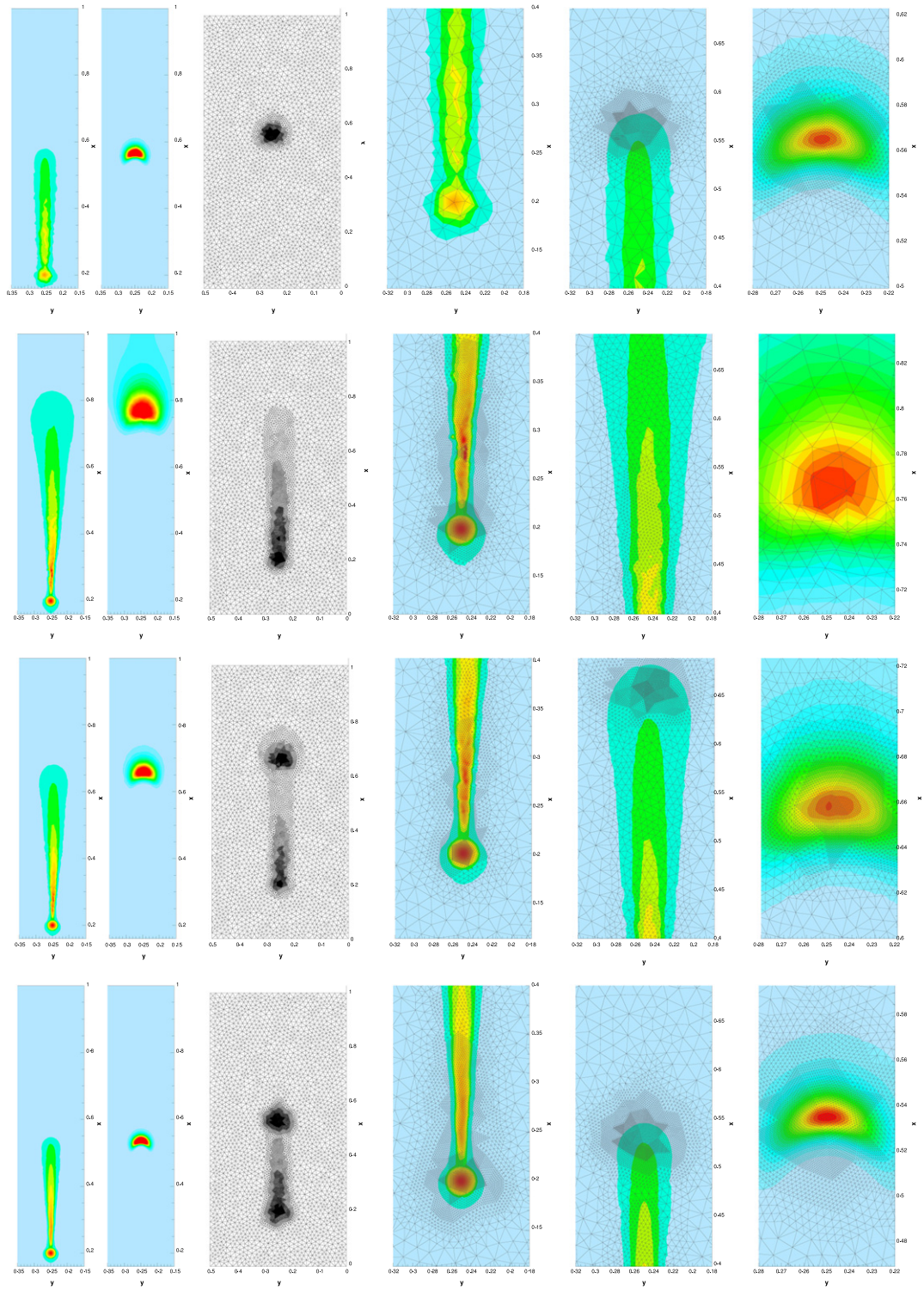

Fig. 6. Criterion based on source terms (first row), criterion based on gradient of electron density (second row), criterion based on source terms and gradient of electron density—Algorithm V1 (third row), Algorithm V2 (fourth row).

Uniform grid refinement. The isolines of net charge density $\rho = e(n_i - n_e)$ are plotted in Fig. 7 (first order scheme) and in Fig. 8 (second order scheme). The grid density is increased from left to right. The grid density influence is shown on 1D plots of electron density n_e along the axis of discharge (line $y = 0.25$) (see Fig. 9).

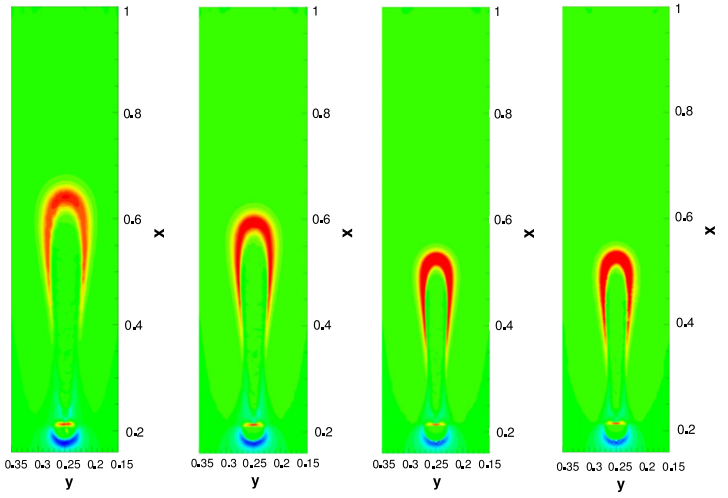

Fig. 7. 1st order, comparison of net charge density computed on different uniformly refined meshes at time $t = 5.25 \cdot 10^{-8}$ s. From left to right: 2 levels, 3 levels, 4 levels, adaptation (4 levels).

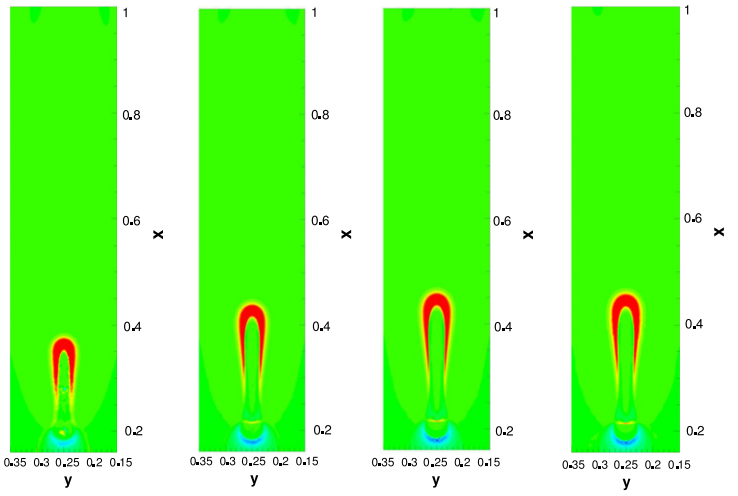

Fig. 8. 2nd order, comparison of net charge density computed on different uniformly refined meshes at time $t = 5.25 \cdot 10^{-8}$ s. From left to right: 2 levels, 3 levels, 4 levels, adaptation (4 levels).

These results confirm that the first order scheme overpredicts the discharge propagation speed. This behavior fully agrees with the conclusion in [10].

The behavior of the method with a second order upwind scheme is different. The position of the streamer head is more stable, the magnitude of electron density slightly increases and the magnitude of net charge slightly decreases when the grid density is increasing. We can also observe a much smaller difference between the results (electron density 1D plots in Fig. 9) on the two last uniformly refined grids compared to the results of the first order scheme. These results show that the second order scheme allows achieving acceptable results with a satisfactory accuracy when using 4 levels of refinement. They also show that first order scheme remains too dissipative and inaccurate despite the high level of refinement used in the grid adaptation algorithm.

This is the first time the authors have observed such a result. Usually the numerical diffusion of an upwind scheme significantly decreases with enough refined grids.

We can also observe that the difference between the first and the second order schemes, although decreasing with increasing grid density, is still important. Both results are plotted together for the grid with 4 levels of refinement in Fig. 10.

Uniformly refined and dynamically adapted grid. Finally we test the accuracy and efficiency of the proposed algorithm of grid adaptation with a second order upwind scheme. The results are compared with those achieved on a uniformly refined grid up to the same fourth level (around $1.2 \cdot 10^6$ grid cells). These comparisons are plotted for the electron density and the net charge density along an axis (see Fig. 11) as well as for the net charge density isolines in Figs. 7 and 8 (the third column – uniformly refined grid, the last column – dynamically adapted grid).

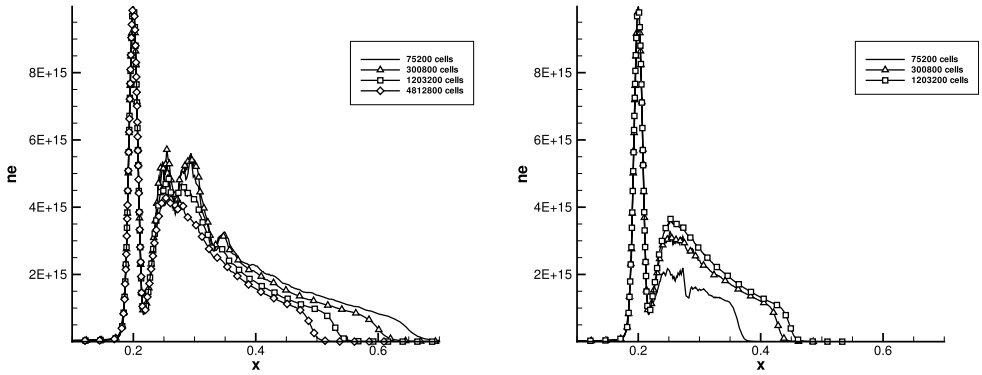

Fig. 9. Comparison of electron density with 1st order (left) and 2nd order (right) schemes, computed on different uniformly refined meshes at time $t = 5.25 \cdot 10^{-8}$ s.t.

Table 3
2nd order: number of cells, nodes and CPU time at time $t = 5.25 \cdot 10^{-8}$ s.

	Cells	Nodes	CPU time
2 levels uniformly refined grid	75 200	37 893	1
3 levels uniformly refined grid	300 800	150 985	8.158
4 levels uniformly refined grid	1 203 200	602 769	58.663
Adapted grid, Algorithm V2	18 636	9 392	1.084

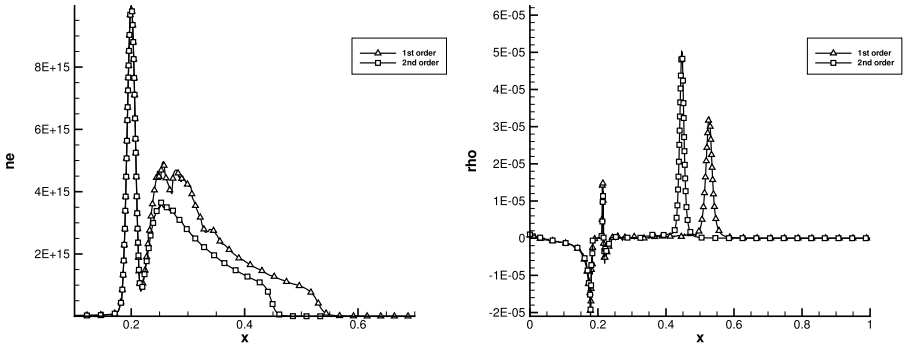

Fig. 10. Comparison of electron density (left) and net charge density (right) for first and second order schemes, grid with 4 levels of refinement.

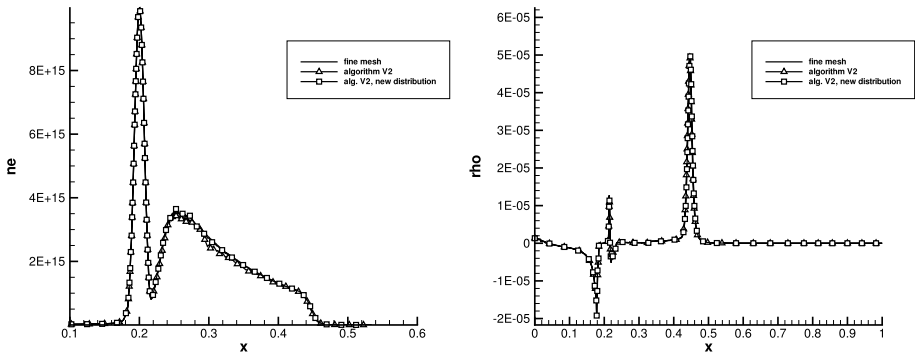

Fig. 11. 2nd order, comparison of electron density (left) and net charge density (right) computed on fine mesh and mesh with dynamic adaptation.

The results are almost identical, which confirms that the proposed grid adaptation algorithm fully conserves the accuracy of the uniformly refined grid. The density of the adapted grid (around 22 000 volumes) confirms the high efficiency of the dynamic grid adaptation algorithm for the considered problem—see Table 3.

6. Conclusions

The paper presents the results obtained with a finite volume solver for the simulation of the propagation of a planar ionization wave front. The solver is based on the Diamond scheme for the diffusive terms, either a first order or a second order upwind Muscle scheme for the estimation of the divergence term of the convection flux, the MKL library for the linear system resulting from Poisson equation and a dynamic mesh adaptation to follow the wave front. The obtained results show first that from a qualitative point of view, the finite volume scheme is able to capture the expected phenomenon of electronic avalanche even with a first order scheme on a relatively poorly adapted grid. The results also show that it is crucial to simultaneously increase the accuracy of the scheme and use a refined grid to reduce the numerical diffusion. This is done with the use of a second order scheme for convection and a dynamically refined grid. The comparison of the CPU time necessary to obtain an accurate result on an adapted grid and on a 4 levels uniformly refined grid, shows that achieving accurate enough simulation of the ionization front propagation with a reasonable computation cost requires using a dynamic mesh adaption, especially when envisaging a simulation for a 3D geometry and streamer ramification phenomena.

Acknowledgments

This work was supported by the Marie Curie Actions of the European Commission in the frame of the DEASE project (MEST-CT-2005-021122).

Grant of Czech Technical University in Prague No. SGS10/244/OHK2/3T/12.

Appendix

Precise formulation of the relation for electron drift velocity v_e [cm $\cdot$ s^{-1}] ($\frac{\|\vec{E}\|}{N}$ [V cm^2]) [7]

$$\begin{aligned}
&\text{for } \frac{\|\vec{E}\|}{N} > 2\cdot 10^{-15}, \qquad \vec{v}_e = -\left[7.4\cdot 10^{21}\cdot\frac{\|\vec{E}\|}{N} + 7.1\cdot 10^{6}\right]\cdot\frac{\vec{E}}{\|\vec{E}\|},\\
&\text{for } 10^{-16} < \frac{\|\vec{E}\|}{N} \le 2\cdot 10^{-15}, \qquad \vec{v}_e = -\left[1.03\cdot 10^{22}\cdot\frac{\|\vec{E}\|}{N} + 1.3\cdot 10^{6}\right]\cdot\frac{\vec{E}}{\|\vec{E}\|},\\
&\text{for } 2.6\cdot 10^{-17} < \frac{\|\vec{E}\|}{N} \le 10^{-16}, \qquad \vec{v}_e = -\left[7.2973\cdot 10^{21}\cdot\frac{\|\vec{E}\|}{N} + 1.63\cdot 10^{6}\right]\cdot\frac{\vec{E}}{\|\vec{E}\|},\\
&\text{for } \frac{\|\vec{E}\|}{N} \le 2.6\cdot 10^{-17}, \qquad \vec{v}_e = -\left[6.87\cdot 10^{22}\cdot\frac{\|\vec{E}\|}{N} + 3.38\cdot 10^{4}\right]\cdot\frac{\vec{E}}{\|\vec{E}\|}.
\end{aligned} \tag{20}$$

Precise formulation for the ratio $\frac{\alpha}{N}$ [cm^2] [7]

$$\begin{aligned}
&\text{if } \frac{\|\vec{E}\|}{N} > 1.5\cdot 10^{-15}, \qquad \frac{\alpha}{N} = 2\cdot 10^{-16}\cdot\exp\left(\frac{-7.248\cdot 10^{-15}}{\|\vec{E}\|/N}\right),\\
&\text{else}, \quad \frac{\alpha}{N} = 6.619\cdot 10^{-17}\cdot\exp\left(\frac{-5.593\cdot 10^{-15}}{\|\vec{E}\|/N}\right).
\end{aligned} \tag{21}$$

References

[1] A. Bourdon, V.P. Pasko, N.Y. Liu, S. Célestin, P. Ségur, E. Marode, Efficient models for photoionization produced by non-thermal gas discharges in air based on radiative transfer and the Helmholtz equations, Plasma Sources Sci. Technol. 16 (2007) 656–678.
[2] C. Montijn, W. Hundsdorfer, U. Ebert, An adaptive grid refinement strategy for the simulation of negative streamers, J. Comput. Phys. 219 (2) (2006) 801–835.
[3] D.S. Nikandrov, R.R. Arslanbekov, V.I. Kolobov, Streamer simulations with dynamically adaptive Cartesian mesh, IEEE Trans. Plasma Sci. 36 (4) (2008) 932–933.
[4] S. Pancheshnyi, P. Ségur, J. Capeillère, A. Bourdon, Numerical simulation of filamentary discharges with parallel adaptive mesh refinement, J. Comput. Phys. 227 (13) (2008) 6574–6590.
[5] W. Min, H. Kim, S. Lee, S. Hahn, A study on the streamer simulation using adaptive mesh generation and FEM-FCT, IEEE Transactions on Magnetics 37 (5, Part 1) (2001) 3141–3144.
[6] A.P. Papadakis, G.E. Georghiou, A.C. Metaxas, New high quality adaptive mesh generator utilized in modelling plasma streamer propagation at atmospheric pressures, J. Phys. D: Appl. Phys. 41 (23) (2008) 234. 019.
[7] R. Morrow, J.J. Lowke, Streamer propagation in air, J. Phys. D: Appl. Phys. 30 (1997) 614–627.
[8] J. Dobes, J. Fort, J. Halama, Numerical solution of single and multi-phase internal transonic flow problems, Internat. J. Numer. Methods Fluids 48 (1) (2005) 91–97.
[9] I. Elmahi, F. Benkhaldoun, R. Borghi, S. Raghay, Ignition of fuel issuing from a porous cylinder located adjacent to a heated wall: a numerical study, Combust. Theory Model. 8 (2004) 789–809.
[10] S. Célestin, Etude de la dynamique des streamers dans l'air a la pression atmospherique, Thesis, E.M2.C CNRS et Ecole Centrale Paris, 2008.

Further reading

[1] E. van Veldhuizen, Electrical Discharges for Environmental Purposes: Fundamentals and Applications, Nova Science Publishers, 2000.
[2] U. Ebert, W. van Saarloos, C. Caroli, Propagation and structure of planar streamer fronts, Phys. Rev. E 55 (1997) 1530–1549.
[3] M. Arrayás, U. Ebert, W. Hundsdorfer, Spontaneous branching of anode-directed streamers between planar electrodes, Phys. Rev. Lett. 88 (2002) 174502. (14).
[4] U. Ebert, D.D. Sentman, Streamers, sprites, leaders, lightning: from micro- to macroscales, J. Phys. D: Appl. Phys. 41 (2008) 230301. (7 pp).
[5] Chao Li, U. Ebert, W. Hundsdorfer, Spatially hybrid computations for streamer discharges: II. Fully 3D simulations, J. Comput. Phys. 231 (2012) 1020–1050.
[6] T. Unfer, J.-P. Boeuf, F. Rogier, F. Thivet, Multi-scale gas discharge simulations using asynchronous adaptive mesh refinement, Comput. Phys. Commun. 181 (2) (2010) 247–258.
[7] D. Bressières, J. Paillol, A. Bourdon, P. Ségur, E. Marode, A new one-dimensional moving mesh method applied to the simulation of streamer discharges, J. Phys. D: Appl. Phys. 40 (2007) 6559–6570.
[8] O. Ducasse, L. Papageorghiou, O. Eichwald, N. Spyrou, M. Yousfi, Critical analysis on two-dimensional point-to-plane streamer simulation using finite element and finite volume methods, IEEE Trans. Plasma Sci. 35 (5) (2007) 1287–1300.
[9] A. Bourdon, D. Bessieres, J. Paillol, A. Michau, K. Hassouni, E. Marode, P. Ségur, Influence of numerical schemes on positive streamer propagation, in: 27 ICPIG, Eindhoven, The Netherlands, July 18–22, 2005.